J Mater Sci (2009) 44:5339–5344
DOI 10.1007/s10853-009-3683-5

FERROELECTRICS

Orientation controlled deposition of $Pb(Zr,Ti)O_3$ films using a micron-size patterned $SrRuO_3$ buffer layer

Ken Nishida · Takashi Yamamoto · Minoru Osada · Osami Sakata · Shigeru Kimura · Keisuke Saito · Masamichi Nishide · Takashi Katoda · Shintaro Yokoyama · Hiroshi Funakubo

Received: 15 March 2009 / Accepted: 12 June 2009 / Published online: 2 July 2009

Abstract Orientation controlled, micron-sized dot-patterned PZT films were grown by metal organic chemical vapor phase deposition (MOCVD), and their crystal structure was evaluated. A micron-size dot-patterned $SrRuO_3$ (SRO) buffer layer was initially prepared by MOCVD through a metal mask on the (111) $Pt/Ti/SiO_2/Si$ substrate. Then, a PZT film was deposited over the entire substrate. Micron-beam X-ray diffraction and Raman spectroscopy indicated that (111)-orientated PZT was prepared on the SRO covered area, while the (100)/(001)-orientated one was directly grown on Pt-covered substrates. The PZT film grown on SRO was thinner than that on the Pt-covered substrate. The estimated ferroelectric property on the center of the dot pattern was larger than that at the circumference by Raman spectroscopy because the strain is accelerated at the center of the dot.

K. Nishida (✉) · T. Yamamoto
Department of Communication Engineering, National Defense Academy, Yokosuka 239-8686, Japan
e-mail: nishida@nda.ac.jp

M. Osada
Advanced Materials Laboratory, National Institute for Materials Science (NIMS), Tsukuba 305-0044, Japan

O. Sakata · S. Kimura
Materials Science Division, Japan Synchrotron Radiation Research Institute, Sayo 679-5198, Japan

K. Saito
Bruker AXS K. K., Yokohama 221-0022, Japan

M. Nishide · T. Katoda
Department of Electronic and Photonic System Engineering, Kochi University of Technology, Kochi 782-8502, Japan

S. Yokoyama · H. Funakubo
Department of Innovative and Engineered Materials, Tokyo Institute of Technology, Yokohama 226-8503, Japan

Introduction

Because $Pb(Zr,Ti)O_3$ (PZT) has excellent ferroelectric, piezoelectric, and pyroelectric properties, applications for non-volatile memory, micro electrical mechanical system (MEMS) devices and infrared sensors have been widely investigated [1, 2]. Among the various applications, MEMS devices, which are typically between 10 and 100 μm [3], are one of the more interesting application fields using PZT. Currently MEMS devices are typically patterned by a dry etching process, e.g., ion beam etching after the PZT film is grown over the entire substrate [4]. However, the damage to the film and substrate by the dry etching process might degrade PZT with respect to the properties and the reliability. Therefore, a benign, direct patterning technology using a direct growth process is strongly demanded. This direct patterning may be realized during film growth either by (i) selective growth of the ferroelectric film in a limited region or (ii) growth of the area where the electrical properties differ. Among these two approaches, selective growth is more difficult because it requires a large difference in the deposition rate between the two regions. In a previous paper, we reported a growth method, which uses a pattern bottom electrode prepared by electron beam (EB) lithography, to fabricate an area consisting of a crystal PZT film and amorphous PZT film with coplanar areas as small as 2 μm [5, 6].

Herein the patterning of the PZT film with different orientations was attempted by inserting a buffer layer. The ferroelectric, piezoelectric, and pyroelectric properties are

polar characteristics, which suggest the films depend strongly on orientation. In fact, the piezoelectric and ferroelectric properties of the PZT films significantly depend on orientation, suggesting the possibility the orientation pattern of the PZT is a response to the pattering of the above properties. PZT films are easily oriented to (111) and (100)/(001). Films are oriented to (100)/(001) when prepared on the widely used (111)Pt/TiO_2/SiO_2/Si substrate by MOCVD with a high deposition rate. However, the orientation can be changed to (111) by inserting a (111)-orientated conductive $SrRuO_3$ (SRO) layer with the same crystal structure and similar lattice parameters as PZT. Based on this background, we prepared a (111)-oriented PZT dot pattern in a (100)/(001)-orientated PZT matrix by creating a dot-patterned SRO buffer layer. The crystal structure of the dot-patterned PZT films was evaluated by X-ray diffraction and Raman spectroscopy.

Experimental

Figure 1 shows the growth sequence. A 5-nm-thick SRO buffer layer was initially prepared on a (111)Pt/Ti/SiO_2/(100)Si substrate (Fig. 1a) through a metal mask placed on the substrate (Fig. 1b). The diameters of the dot pattern in metal mask were 200 and 500 μm. Then the PZT film was deposited over the entire substrate (Fig. 1c). PZT films and SRO buffer layers were deposited at 650 and 600 °C, respectively, by metalorganic chemical vapor deposition (MOCVD). $Pb(C_{11}H_{19}O_2)_2$-$Zr(O•t\text{-}C_4H_9)_4$-$Ti(O•i\text{-}C_3H_7)_4$-O_2 and $Sr(C_{11}H_{19}O_2)_2(C_8H_{23}N_5)_2$-$Ru(C_7H_{11})(C_7H_9)$-$O_2$ were the respective source systems for the PZT film and SRO buffer layer growth. The Zr/(Zr + Ti) and Pb/(Pb + Zr + Ti) ratios of the PZT film were maintained at 0.40 and 0.50, respectively [7]. Herein we focused on PZT films grown on SRO buffer layers with a 500 μm dot pattern because the spatial resolution of the X-ray beam cannot sufficiently evaluate a 200 μm-dot-patterned PZT film.

The crystal structure and the orientation of the deposited films were characterized using micron-beam X-ray diffraction (Bruker AXS, Discovery D8). The X-ray beam was focused on an approximately 50-μm-diameter on the sample surface. A two-dimensional detector was used in this system, and the $\theta-2\theta$ diffraction pattern of the sample was obtained without moving the goniometer. Additionally, transmission electron microscopy (TEM) of H-8000 (HITACHI) with an acceleration voltage of 300 kV was used to evaluate the microscopic structure. The film thickness was measured using a surface-profile measuring system (DEKTAK 3). X-ray fluorescence was measured to estimate the distribution of film thickness using X-ray diffraction of synchrotron radiation (SPring-8, BL13XU)

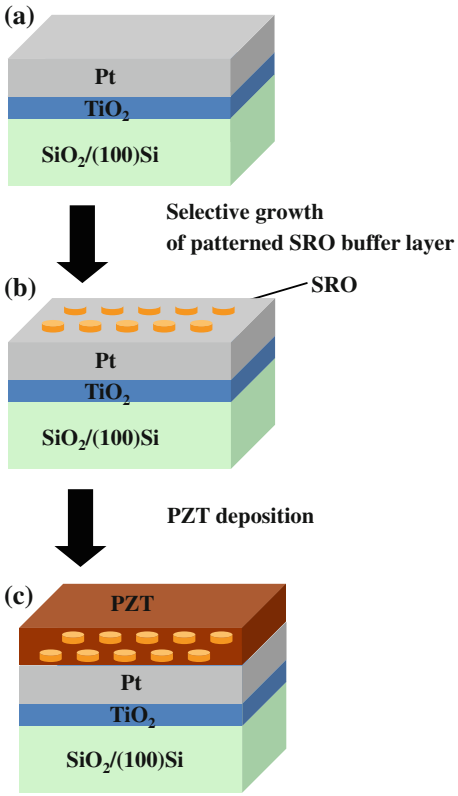

Fig. 1 Growth sequence of a dot-patterned PZT film: **a** (111)Pt/TiO_2/SiO_2/Si substrate, **b** deposition of dot-patterned SRO buffer layer, and **c** overgrowth of the PZT film

[8] The incident size of the X-rays was approximately a 20 μm square on the sample surface.

The quality and ferroelectric property of the PZT film were estimated by Raman spectroscopy. Micro Raman spectroscopy was carried out using SYSTEM 1000 (RENISHAW) with a super noch plus filter in the back-scattering configuration. A 514.5-nm-Ar^+ laser was used as the excitation source, and the laser power at the sample was approximately 2 ∼ 3 mW. Raman spectra were collected from the sample surface with a spatial resolution less than 1 μm using a 200 objective to focus. The spectrometer was calibrated using the silicon Raman mode and laser plasma lines. The resolution of the phonon frequency measurement was better than 0.1 cm^{-1}. The samples were scanned in 0.1 μm steps using a motorized XY stage to produce maps of the phonon frequencies and their intensities. To improve the signal-to-noise (S/N) ratio, measuring time was fixed at 1 min per point.

Results and discussion

Figure 2a shows the optical microscopic image of the sample. Dot patterns were formed on the sample surface.

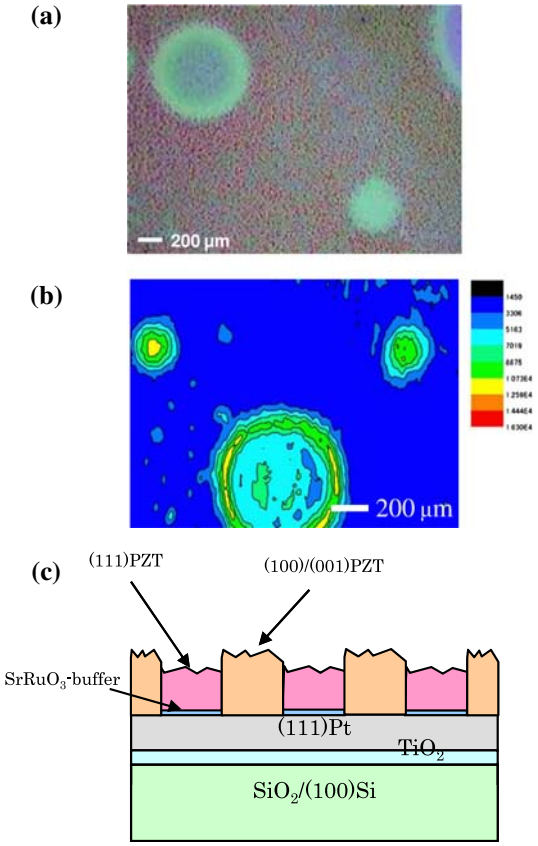

Fig. 2 **a** Optical micrographs of the dot-patterned PZT film, **b** mapping image of the fluorescent X-ray of the Pt-Lα line using synchrotron X-ray diffraction, and **c** schematic drawing of the cross section of the structure

Figure 2b shows the X-ray florescent mapping pattern of Pt-Lα. The peak intensity of the florescence was high in the dot-circle, indicating that the thickness of the overgrowth PZT film was thinner than that on the outside, as schematically shown in Fig. 2c, which agrees with the surface profiler results. Despite coplanar and simultaneous growth, the film thickness of PZT on the SRO buffer layer was about half that on the Pt bottom electrode, i.e., the film thickness of PZT on the SRO buffer layer was about 200 nm, while the thickness on the Pt bottom electrode was 400 nm. This difference in film thickness along with the film orientation is discussed below.

Figure 3a shows the XRD $\theta-2\theta$ patterns measured along the *Y*-direction using optical microscopy. The PZT film was oriented to (111) on the SRO buffer layer, whereas it was oriented to (001)/(100) when directly deposited on Pt. These film orientations are consistent with previous reports [5, 6]; the growth rate of (100)/(001)-oriented film on (100) $SrTiO_3$ (STO) is twice as fast as that of the (111)-oriented one on (111) STO [9]. The difference in film thicknesses in the dot pattern shown in Fig. 2 can be explained by the different deposition rates with the film orientation. The lattice parameters of the *a*- and *c*-axis at the center of dot pattern and at the outer circumference of dot pattern that had (111) orientation were 3.918, 4.066 and 3.919, 4.064 Å, respectively. The *c*-axis at the center of dot pattern was slightly larger than that of the outer circumference of dot pattern and the *a*-axis at the center of dot pattern was slightly smaller than that of the outer circumference of dot pattern. On the other hand, the lattice parameters of the *a*- and *c*-axis at the outside dot pattern that had (001)/(100) orientation were almost 3.919 and 4.064 Å, respectively. It is considered that the strain was maintained in the PZT film and that at the center of the dot pattern was larger than that at the outer circumference, while the strain was almost uniform at the outside dot pattern.

Figure 4a, b shows the TEM images of PZT films on the SRO buffer layer and for films directly on Pt bottom electrode, respectively, as well as the electron beam diffraction patterns. PZT films deposited on the SRO buffer layer had a relatively flat surface, and were oriented to the (111) direction (Fig. 4a). On the other hand, PZT films directly deposited on Pt consisted of grains with irregular shapes,

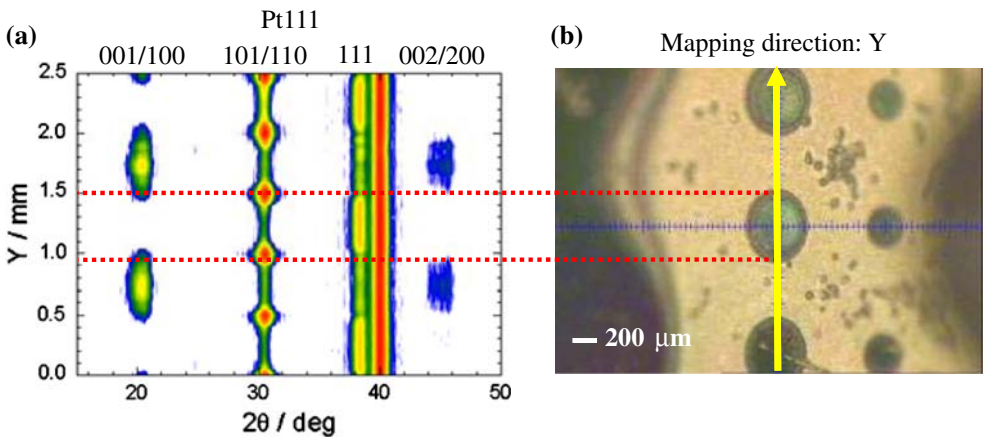

Fig. 3 **a** Intensity integration map of XRD using Micro-beam X-rays and **b** picture of the dot-patterned PZT film from a CCD camera

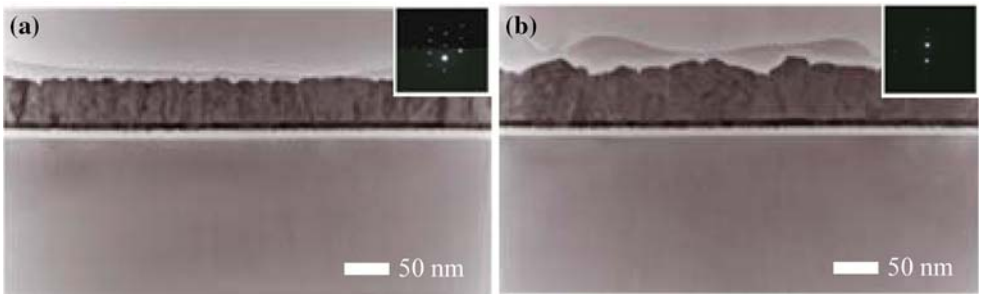

Fig. 4 Cross-sectional TEM images and electron diffraction patterns of **a** PZT film on the SRO buffer layer (center of the dot pattern) and **b** PZT film on Pt (outside of the dot pattern)

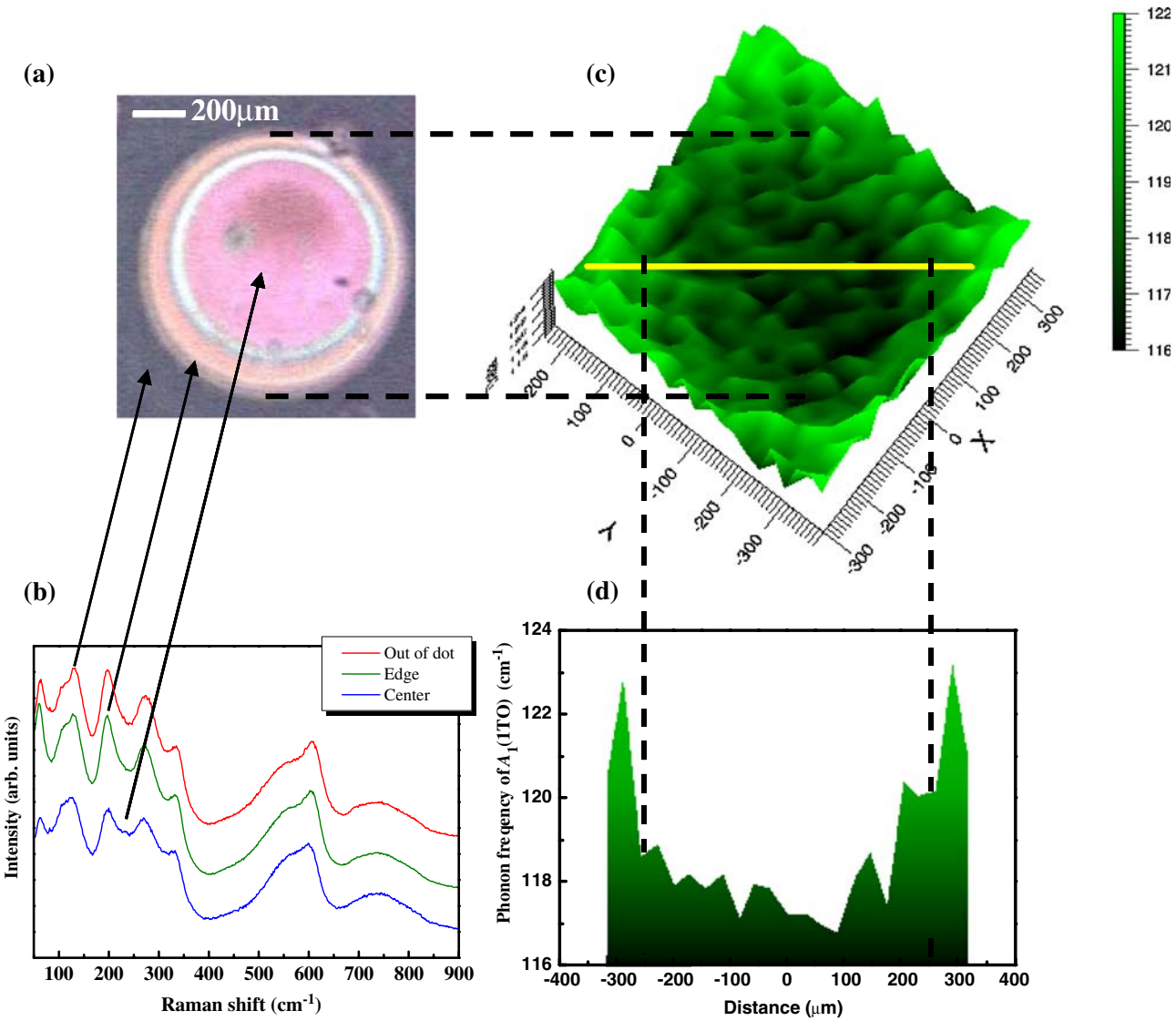

Fig. 5 **a** Picture of the dot-patterned PZT film from a CCD camera and **b** parallel polarized Raman spectra at center, edge, and the outside the dot of dot-patterned PZT. Measurement points are indicated by arrows in **a**. **c** Raman shift map of A_1(1TO)-mode for the dot-patterned PZT, and **d** its cross-section

which made a rough surface (Fig. 4b). The electron diffraction patterns indicated a (100)/(001) orientation, which agrees with the XRD results. Hence, the data indicate that a PZT film with different coplanar orientations was successfully grown using a patterned SRO buffer layer on the Pt bottom electrode.

Figure 5b shows the parallel polarized Raman spectra from the center, edge, and about 500 μmΦ outside the dot-patterned PZT, as denoted in Fig. 5a. The parallel *yy*-polarization configuration yields only A_1-symmetry modes [10, 11]. The Raman spectra exhibited intense A_1-symmetry phonons, and the spectrum for each part of the dot-patterned PZT film indicates a typical tetragonal PZT. Additionally, similar to the XRD data (Fig. 3a), a second phase was not observed. The Raman peaks were shifted, indicating changes in the crystal orientation and strain in the crystal. The peak position A_1-symmetry modes shifted to a lower wavenumber when the measured position changed from the center to outside the dot pattern. This corresponds to an orientation change from (111) to (001)/(100), which is consistent with previous reports [12, 13].

For a more detailed investigation of the film orientation and strain distribution in same film orientation area, Raman mapping of the A_1(1TO) mode was measured. Figure 5c shows the results. The orientation of the PZT film changed from (111) to (001)/(100) through the (101)/(110) orientation from the center to outside the dot pattern, which agrees with the XRD results (Fig. 3a). The frequency of the A_1(1TO)-mode at the center of the dot pattern was slightly higher than that of the edge of the dot pattern (Fig. 5d), even if the PZT film on the dot pattern had the same (111) orientation, indicating the strain in the PZT film is larger at the center of the dot pattern than at the edge of the dot pattern.

The volume fraction of the *c*-domain and polarization property were characterized by Raman spectroscopy. The intensity of the A_1(1TO) soft mode was applicable as a probe for the domain distribution and polarization property [14] because the Raman peak intensity of the A_1(1TO) soft mode is proportional to the *c*-domain volume and saturation polarization [15]. The ferroelectric property of the dot-patterned PZT film was predicted using its relationship with the intensity of the A_1(1TO) soft mode [16].

To obtain two-dimensional information about the ferroelectricity in the dot-patterned PZT, the mapping measurements of Raman spectroscopy were carried out. Figure 6a shows the Raman intensity map of the A_1(1TO) soft mode. The ferroelectricity was large when the peak intensity of the A_1(1TO) soft mode was high. In Fig. 6a, the polarization property changes according to the film orientation. The (001)/(100) oriented area, which is outside the dot pattern, consisted of the *a*- and *c*-domains. From the intensity of the estimated A_1(1TO)-mode, the *c*-domain volume was approximately 60%. The estimated saturation polarization of the PZT film orientated to (001)/(100) was around 40–50 μC/cm^2, while that of (the 111) orientated area, which is the center of the dot pattern, was approximately 60% of the saturation polarization of (001)/(100). These are typical saturation polarization values for a PZT film with

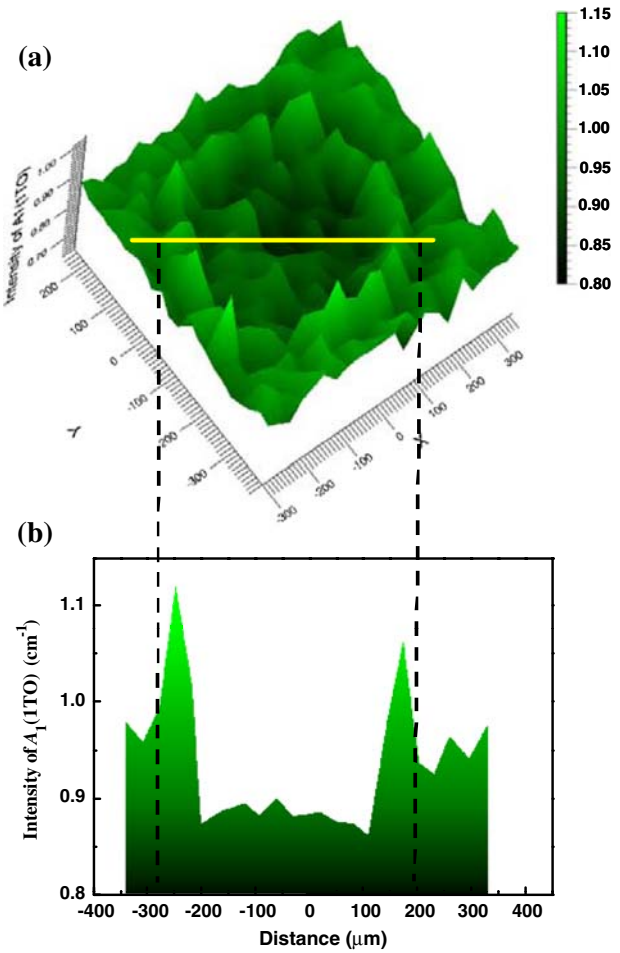

Fig. 6 **a** Raman intensity map of the A_1(1TO)-mode for the dot-patterned PZT and **b** the cross-section of Raman intensity map along line shown in **a**

different orientations. The intensity of the A_1(1TO)-mode at the center of the dot pattern was slightly higher than that at the outer circumference of the dot pattern (Fig. 6b), indicating that the saturation polarization varied in the dot pattern. The saturation polarization at the center of the dot pattern was larger than that of at the outer circumference. Hence, compressive strain is larger at the center of dot pattern. These results were agreed with the results of XRD as shown in Fig. 3.

The micro-dot-patterned PZT film with different saturation polarizations could be fabricated using a coplanar SRO buffer layer. This is a very simple method, which does not require a complicated device process; thus, is a useful method for MEMS devices fabrication.

Conclusion

A dot-patterned PZT film, which was fabricated using a metal mask by MOCVD, was obtained on the SRO dot

pattern. A (111)-orientated PZT film was successfully grown on the SRO covered area, while a (100)/(001)-orientated one was directly grown on the Pt substrate. The film orientation, crystallinity, and ferroelectric property were estimated using XRD and Raman spectroscopy, which are useful evaluations methods with two-dimensional spatial resolution. Although the dot-patterned PZT film was coplanar, it simultaneously displayed different film orientations and ferroelectric properties. Thus, this method has great potential for fabricating MEMS devices through a simple device process.

References

1. Scott JF, de Araujo CAP (1989) Science 246:1400
2. Auciello O, Scott JF, Ramesh R (1989) Phys Today 51:22
3. Muralt P (2000) J Micromech Microeng 10:136
4. Spearing SM (2000) Acta Mater 48:179
5. Yokoyama S, Takahashi K, Okamoto S, Nagai A, Minamidate J, Saito K, Ohashi N, Haneda H, Sakata O, Kimura S, Nishida K, Katoda T, Funakubo H (2006) Jpn J Appl Phys 45:5102
6. Takahashi K, Oikawa T, Saito K, Kaneko S, Fujisawa H, Shimizu M, Funakubo H (2002) Jpn J Appl Phys 41:5376
7. Yokoyama S, Ozeki T, Oikawa T, Funakubo H (2002) Jpn J Appl Phys 41:6705
8. Sakata O, Furukawa Y, Goto S, Mochizuki T, Uruga T, Takeshima K, Ohashi H, Ohata T, Matsushita T, Takahashi S, Tajiri H, Ishikawa T, Nakamura M, Ito M, Sumitani K, Takahashi T, Shimura T, Saito A, Takahashi M (2003) Surf Rev Lett 10:543
9. Yokoyama S, Ozeki T, Oikawa T, Funakubo H (2003) Integ Ferro 59:1429
10. Lee S-H, Jang HM, Sung HH, Yi H (2002) Appl Phys Lett 81:2439
11. Lee S-H, Jang HM, Cho SM, Yi G-C (2002) Appl Phys Lett 80:3165
12. Loudon R (1964) Adv Phys 13:423
13. Merten L (1968) Phys Status Solidi B 25:125
14. Nishida K, Osada M, Wada S, Okamoto S, Ueno R, Funakubo H, Katoda T (2005) Jpn J Appl Phys 44:L827
15. Okamoto H, Asano G, Oikawa T, Saito K, Funakubo H (2003) Appl Phys Lett 82:4761
16. Osada M, Nishida K, Wada S, Okamoto S, Ueno R, Funakubo H, Katoda T (2005) Appl Phys Lett 87:232902